

ULRR

Removal of ortho-phosphate from aqueous solution by adsorption onto dolomite

Item Type	Article
Authors	Mangwandi, Chirangano;Albadarin, Ahmad B.;Glocheux, Yoann;Waler, Gavin M.
Citation	Journal of Environmental Engineering;2 (2), pp. 1123-1130
Publisher	Elsevier
Download date	2026-06-10 02:49:03
Item License	https://creativecommons.org/licenses/by-nc-sa/1.0/
Link to Item	https://hdl.handle.net/10344/7255

26 **Abstract**

27 An experimental study on the adsorption of phosphate onto cost effective fine dolomite powder
28 is presented. The effect of solution pH, solution ionic strength and adsorption isotherm were
29 examined. The adsorption of phosphate was pH dependent and phosphate adsorption favoured
30 acidic conditions, with a maximum uptake of 377. mg g⁻¹ at pH 2. The adsorption was
31 significantly influenced by solution ionic strength indicating outer-sphere complexation
32 reactions. The experimental data further indicated that the removal of phosphate increased
33 with increase in the ionic strength of solution. The experimental data was modelled with
34 different isotherms, such as: Langmuir, Freundlich and Redlich–Peterson isotherms; on
35 analysis it was found that the Redlich–Peterson isotherm depicted the equilibrium data
36 accurately. The overall kinetic data fitted very well the pseudo first-order rate model.

37

38

39

40

41

42

43

44

45

46

47

48

49

50

51 **1. Introduction**

52 Phosphate is one of the most important nutrients essential for plant growth and modern
53 agricultural methods [1]. Phosphate is discharged to water by various human activities;
54 industrial and agricultural applications. The extensive discharge of phosphate into surface
55 water can cause eutrophication, and thus lower the water quality [2]. Therefore, effective
56 phosphate recovery techniques will prevent the pollution of water environment and overcome
57 the resource deficiency issue. The removal technologies for aqueous phosphate or phosphorous
58 from contaminated waters include: crystallization, chemical precipitation and biological
59 removal. In phosphate removal investigations regarding crystallization [3-5], a number of
60 materials such as sand and Ca-phosphate crystals were utilized as seeding materials to initiate
61 and improve phosphate recycling and precipitation. However, a crystallization method requires
62 complicated and precise control of the operating conditions [1, 6]. Chemical precipitation and
63 biological removal have other disadvantages such as: the cost of chemicals, substantial
64 additional sludge production and phosphorus release in the sludge treatment [7].

65 Adsorption is becoming an increasingly important process for the elimination of
66 contaminants from waste waters [8, 9]. A detailed review of P nutrient removal and recovery
67 technologies was given by Morse [10]. The adsorption technique offers a number of advantages
68 over the other techniques for instance it allows use of low cost materials for remediation of
69 contaminated waste water; the process scale-up is easy and low operational costs [11]. Several
70 studies on the removal of phosphorus/ phosphate from contaminate waters using the adsorption
71 method have been given in literature [12-17]. Dolomite [$\text{CaMg}(\text{CO}_3)_2$], a material that is
72 existing abundantly and cheaply worldwide [18] is the subject of attention for more than six
73 decades [11]. Despite a relatively low specific surface area ($\sim 1.50 \text{ m}^2 \text{ g}^{-1}$) [19], dolomite still
74 shows some good adsorption properties. Karaca et al. carried out a comparison between
75 calcinated dolomite and raw dolomite in terms of capacity of phosphate removal from aqueous

76 solution [20]. Authors reported that the phosphate capacity increased with an increased in the
77 solution pH at a solid-liquid ratio 2.0 g/L, adsorption temperature 20 °C and ionic strength 0.0
78 M. Authors reported that the Phosphate removal decreased with increasing temperature and
79 slightly increased with increasing of pH. It was suggested that the main mechanisms for
80 adsorption of phosphate on dolomite could be both physical interactions and chemi-sorption.

81 This research was carried out to investigate the removal of phosphate from aqueous
82 solutions by adsorption onto low cost dolomite materials, through equilibrium and kinetic
83 studies. This research differs from the earlier studies [20, 21] in a number of ways. Firstly,
84 higher initial concentrations of phosphate solution were used to match the typical phosphate
85 levels in slurries from anaerobic digestion plants. Unlike in the previous research reports, where
86 coarse particle of adsorbent were used, this research used very fine raw dolomites powder as
87 this size allows further processing of the powder after adsorption for use as soil-conditioner
88 [22-24]. Secondly, this paper studies the effect of solution ionic strength which has not been
89 studied before. Further insights on the mechanism and nature of the adsorption process were
90 gained by applying appropriate equilibrium and kinetic models to the experimental data.

91 **2. Materials and Methods**

92 **2.1 Chemicals**

93 Calcium phosphate monobasic manufactured and supplied by Aldrich – Chemical Co. Ltd,
94 UK was used as the source of phosphate ions. The adsorbent used in this research was fine
95 dolomite supplied by Kilwaughter Chemical Company, UK, which had a particle size between
96 50–100 µm. The fine dolomite in this study has been tested for adsorption experiments without
97 any pre-treatment. Solutions of 1M of HCl and NaOH were used for the manual control of pH
98 (pH meter, Thermo Fisher scientific-Singapore). The electrolyte used to modify the ionic
99 strength in the adsorption experiments was NaCl.

100 **2.2 Equipment**

101 A XRD analysis was performed to examine the crystalline nature of the fine dolomite
102 sample (Wide angle X-ray diffraction using a Philips analytical X'pert pro diffractometer).
103 The surface structure of the fine dolomite was explored with Fourier Transform Infrared
104 Spectroscopy (FT-IR), to illustrate the change in the functional groups of the dolomite surface
105 before and after adsorption. The structural ordering of the fine dolomite was analyzed by
106 scanning electron microscopic (SEM), using a JEOL-JSM 6400 scanning microscope. For
107 batch equilibrium studies, samples have been regularly shaken (mechanical shaker, GerhardT
108 type LS 5) for 7 days at 100 rpm and 20 °C. The initial and final concentrations of the nutrients
109 were measured by inductive couple plasma (ICP-OES, Optima 4300 DV, 16 Perkin Elmer,
110 USA). The surface area and the cumulative pore size distribution of the dolomite powder were
111 measured using a mercury porosimetry (PoreMaster[®], QuantaChrome Instruments).

112 **2.3 Adsorption Experiment**

113 The influence of solution pH on adsorption capacity was investigated by adding 0.2 g of
114 adsorbent to 250 mL bottle jars containing 50 mL solutions solution ($C_0 = 1000$ mg P/L) at
115 room temperature (20 °C). The experiment was performed using solutions at various pH values:
116 2 to 10. The influence of ionic strength on the adsorption of phosphate onto dolomite was
117 examined by altering the initial phosphate concentrations 100 and 2000 mg/L in the existence
118 of NaCl salt, at three altered concentrations 0.05, 0.1 and 0.3 M. This value was selected based
119 on the average ionic strength values used in phosphate adsorption research paper reported in
120 literature [25, 26]. Batch equilibrium studies were performed by adding 0.2 g of adsorbent to
121 250 mL bottle jars containing 50 mL solutions of altered initial concentrations (100–2000 mg
122 P/L) and agitated at 100 rpm using mechanical shaker, GerhardT type. The equilibrium time
123 for all experiments was 7 days. After the adsorption equilibrium was achieved, solutions were
124 filtered to remove the fine dolomite, transferred into polythene tubes and diluted prior to

125 analysis. The amount of phosphate adsorbed at equilibrium, q (mg/g), which corresponds to
126 the difference in phosphate concentration in the solution before and after adsorption was
127 calculated using the following equation:

$$q = \frac{V(C_o - C_e)}{m_s} \quad (1)$$

128 where C_o and C_e (mg P/L) are the concentration of nutrient at initial and equilibrium,
129 correspondingly, V is the volume of the solution (L) and m_s is the mass of dolomite (g).

130 For kinetic studies, 1.0 g of the adsorbent material was contacted with 250 mL of phosphate
131 solution with initial concentration 1000 mg P/L and stirred by a magnetic stirrer. Samples were
132 taken at ordinary time intervals. The solution pH was not adjusted for this set of experiments;
133 the solution had an initial pH 4. However, 100 mg.L⁻¹ of NaHCO₃ was added in solutions used
134 in adsorption experiments as a pH buffer. The phosphate uptake at any time q_t (mg/g) was
135 calculated using Eq. (1). To compare the capability of each adsorption isotherm and kinetic
136 model to predict the experimental data, a standard deviation is calculated as follows [27-30];

$$SD = \sqrt{\frac{\sum ((q_{t,\text{exp}} - q_{t,\text{mod}}) / q_{t,\text{exp}})^2}{N - 1}} \quad (2)$$

137 where N is the number of data points, $q_{t,\text{exp}}$ and $q_{t,\text{mod}}$ are the measured and calculated
138 concentrations of adsorbate in solid phase respectively.

139

140 3. Results and Discussion

141 3.1 Characterization of Adsorbent

142 The performance of an adsorption material is influenced by the porosity and surface area
143 available for adsorption. Fig. 1 shows the cumulative pore size distribution of the dolomite

144 powder. It was found that the powder median pore-diameter, d_{50} , of 15 μm . This means that
145 pores of size of about 15 μm or less contribute to about 50% of the pore surface area; the
146 adsorbent can therefore be described as being macroporous. The surface area of the dolomite
147 was 0.146 m^2/g measured by the mercury porosimetry. Semi-quantitative analysis of the data
148 given in Table 1 indicates that the main component is calcite which is about 68%. The
149 comparison between the XRD profiles before and after adsorption with phosphate is shown in
150 Fig. 2. The X-Ray Diffraction analysis undertaken on the dolomite powder presented in Fig.
151 2a illustrates that the main components are calcite, dolomite, quartz and periclas. It can be
152 noted from Fig. 2b that adsorption of phosphate has the effect of shifting the peaks to the left.
153 There is also a significant reduction in the main calcite peaks which suggests that there may be
154 some dissolution of carbonate during the experiment. The phosphate adsorption onto dolomite
155 results in the appearance of a sharp new peak at around 2θ of 11° and an increase in the
156 intensity of the peak $\sim 21^\circ$ (see Fig. 2b). This phenomena indicate the formation of $\text{Mg}_3(\text{PO}_4)_2$
157 and $\text{Ca}_3(\text{PO}_4)_2$ and the crystalline nature of these precipitates [31].

158 FTIR analysis undertaken on the dolomite before and after adsorption of phosphate is
159 presented in Fig. 3. A broad and intense band of O–H stretching vibration around 3500–3300
160 cm^{-1} and a band around 1700 cm^{-1} (O–H bending vibration) specified the existence of
161 coordinated water molecule [32]. The existence of silicate phases (Si–O vibrations) can be seen
162 at 1040 cm^{-1} and the band at 1437.1 cm^{-1} may be assigned to CO_3^{2-} group [11]. There is a
163 noticeable increase in the intensity of –OH group, which can be attributed to the attraction
164 between the protonated –OH groups and phosphate ions i.e., electrostatic attraction. The
165 reduction of CO_3^{2-} group band may indicate the substitution of carbonates on the dolomite by
166 phosphate ions. There is also a corresponding increase in the bands associated with phosphate
167 group at frequencies of 471, 566, 604 and 961 cm^{-1} . The new band at 1050 cm^{-1} can be due to
168 the bending vibration of adsorbed phosphate [33]. The FT-IR spectra showed that calcium

169 phosphate precipitates were formed and phosphate fixation with Mg^{2+} in amorphous form can
170 be predicted. The fine dolomite surface topography before and after phosphate adsorption was
171 examined by SEM, and the results are revealed in Fig.4. In fresh dolomite particles (Fig. 4a),
172 the particles are covered with amorphous fuzzy materials, whereas the surface of the loaded
173 fine dolomite is almost crystalline. The presence of fines at the surface of the samples
174 underlines the very brittle nature of the materials used in the study. The crystalline structure
175 reveals the formation of $Ca_3(PO_4)_2$ and/or $Mg_3(PO_4)_2$ through surface precipitation [34].

176 **3.2 Effect of solution pH**

177 The effect of altering the pH of the solution on the adsorption of phosphate ions onto dolomite
178 adsorbent after 7 days is shown in Fig. 5. The adsorption capacity decreased considerably with
179 increasing of solution pH from 2 to 10. This clearly shows that the adsorption of phosphate
180 ions onto fine dolomite is pH dependent and that the phosphate adsorption favoured acidic
181 conditions, with a maximum uptake of 227.3 mg P/g at pH 2. $H_2PO_4^-$ and HPO_4^{2-} are dominant
182 phosphate species in the solution under the tested pH range [35]. At low pH (i.e. $pH < 4$), the
183 adsorbent surface is the positively charged and favours the adsorption of phosphate ions. The
184 point of zero charge (PCZ) of dolomite was previously determined as 8.55 [11]. Similar trends
185 have been found by other several studies showing dependence of sorption of phosphate on pH
186 of the solution [15, 16, 36].

187 On the other hand, increasing the pH decreased the uptake of phosphate on fine
188 dolomite. It is known that the adsorption of oxyanion onto negatively charged adsorbent
189 surface sites is not favoured due to the electrostatic repulsion [37]. The reduction in the capacity
190 of adsorption with an increase in pH is attributed to competition for the positively charged sites
191 on the adsorbent as high pH. As the pH of the solution increases the OH^- species in the
192 solution increases, these compete for positive sites on the adsorbent surface with the target
193 PO_4^{3-} ions and the amount of adsorption is consequently dropped. Dolomite is mainly

194 composed of MgCO_3 and CaCO_3 . Dolomite surface is rough, which perhaps results in
195 chemisorption of phosphate ions attributed to increasing the possibility of solid contact. In
196 addition, at low pH values, this could increase the adsorption of phosphate onto dolomite in
197 the form of $\text{Mg}_3(\text{PO}_4)_2$ and $\text{Ca}_3(\text{PO}_4)_2$ [11, 21]. Surface precipitation of P with Ca to form
198 corresponding phosphates of discrete solid phase, is a possible mechanism for phosphate
199 removal onto fine dolomite [38].

200 **3.3 Effect of Ionic Strength**

201 Fig. 6 shows the effect of ionic strength on the removal of phosphate ions by fine
202 dolomite at two different initial phosphate concentrations (100 and 2000 mg/L). It was found
203 that as the ionic strength increased from 0.05 to 0.3 M, the adsorption of phosphate increased
204 from 58.3 to 81.4 mg P/g and from 371.0 to 583.1 mg P/g for phosphate initial concentrations
205 100 and 2000 mg P/L, respectively. The ionic strength dependence indicates an outer-sphere
206 complexation reactions [39]. Similar results have been described by Zhang et al. (2009) [35]
207 for phosphate adsorption from water by a Fe–Mn binary oxide adsorbent.

208 The Na ions may enhance the adsorption of phosphate by reducing the repulsion
209 between the phosphate ions adsorbed on the surface. It can also be observed from Fig. 6 that
210 for high initial concentration of P, increasing the ionic strength from 0.05 M to 0.1 M results
211 in an increase in the q_e (almost doubles) though a further increase to 0.3 M results in a slight
212 reduction in the q_e value. This may be due to the high concentration of Cl^- ions which will act
213 as competitive ions for the adsorption sites. Antelo et al. (2005) [40] indicated that the salt
214 effect was stronger and the adsorption increased by increasing NaCl concentration at solution
215 pH 6. The increase in phosphate uptake with increase of NaCl concentration maybe also due
216 to the macromolecular phosphate configuration [41]. The negatively charged phosphate
217 macromolecules are screened and therefore the phosphate molecules wound up like

218 unsystematic coils. In this more compressed arrangement, more phosphate can be sorbed onto
219 a given area of adsorbent surface.

220 3.4 Equilibrium modelling

221 3.4.1. Freundlich Isotherm

222 The Freundlich isotherm explains a particular phenomena when the adsorption takes
223 place on a heterogeneous surface [42]. The Freundlich isotherm model is given in Eq. 3:

$$q_e = K_F C_e^{1/n} \quad (3)$$

224 where K_F and n are the Freundlich constants. The Freundlich isotherm constants obtained
225 from non-linear regression fitting are revealed in Table 2.

226 3.4.2. Langmuir Isotherm

227 The Langmuir isotherm described an adsorption process taking place at specific homogenous
228 sites with a uniform distribution of energy within the adsorbent surface.

229 The Langmuir isotherm is given in Eq. 4:

$$q_e = q_{\max} \left[\frac{bC_e}{1+bC_e} \right] \quad (4)$$

230 where Langmuir constant a_L (L/mg) is corresponds to the adsorption energy and $K_L = q_{\max} \times$
231 a_L ; q_{\max} is the Langmuir monolayer capacity.

232 The Langmuir constants can be employed to calculate, R_L , the separation factor which is given
233 by:

$$R_L = \frac{1}{1 + (K_L)C_o} \quad (5)$$

234 A value of R_L between 0 and 1 indicates adsorption is favourable, while $R_L > 1$ indicates an
235 unfavourable adsorption process [43].

236 3.4.3. Redlich & Peterson Isotherm

237 Redlich and Peterson isotherm which can explain the adsorption process over a wide
238 range of concentrations integrates some features of both the Langmuir and Freundlich
239 isotherms as given in Eq. 6:

$$q_e = \frac{K_R C_e}{1 + a_R C_e^\beta} \quad (6)$$

240 where a_R (L/mg) and β are the isotherm constants and K_R is the modified Langmuir
241 constant (L/g). Commercial software (SigmaPlot version 11.0, Systat Software Inc.) was used
242 to perform non-linear regression fits of isotherm equations.

243 To confirm the previous findings, the influence of ionic strength on the adsorption of
244 phosphate onto fine dolomite was also studied at six different concentrations in order to obtain
245 adsorption equilibrium isotherms after 7 days contact time. Langmuir, Freundlich and Redlich–
246 Peterson models were employed to describe the experimental data and results are revealed in
247 Table 2 and Fig. 7 (For 0.0 M NaCl only). It is apparent from Table 2 and Fig. 7 that Redlich–
248 Peterson isotherm provides the best fit to the experimental data at all NaCl concentrations
249 studied with R^2 values higher than 0.957. Also, apart from at 0 M NaCl concentration, the
250 values of standard deviation for Redlich–Peterson isotherm were lower than those for Freundlich
251 and Langmuir isotherms at all experimental conditions studied. However, the Freundlich
252 isotherm constant, n , which is an indication of adsorption intensity was higher than unity
253 suggesting that the adsorption of phosphate onto fine dolomite is favourable [44]. The
254 separation factor, R_L , values for the adsorption of phosphate onto dolomite were in the range
255 of 0.088–0.173 (Table 2) which indicates that the adsorption is a favourable process.

256 3.5. Adsorption Kinetics

257 The pseudo-first-order and pseudo-second-order kinetic models were fitted to the kinetic
258 data. The intra-particle diffusion and Elovich models were also employed to find out the
259 adsorption diffusion mechanisms. The SD values for the different models are given in Table
260 3.

261 The adsorption kinetics may be explained by pseudo first order model [11];

$$q_t = q_e (1 - e^{-k_1 t}) \quad (7)$$

262 This can also be given in a linear form as;

$$\ln(q_e - q_t) = \ln(q_e) - k_1 t \quad (8)$$

263 where k_1 is the rate constant for first order adsorption (min^{-1}). The linear plot of $\ln(q_e - q_t)$
264 versus t is shown in Fig. 88 (a).

265 The kinetic data for adsorption can also be explained by the pseudo-second-order equation
266 which is expressed as;

$$q_t = \frac{q_e^2 k_2 t}{1 + q_e k_2 t} \quad (9)$$

267 The linear form of the pseudo second order equation can be given as;

$$\frac{t}{q_t} = \frac{1}{k_2 q_e^2} + \frac{1}{q_e} t \quad (10)$$

268 where k_2 (g/mg h) is the adsorption rate constant for the second-order model. q_e is the
269 equilibrium adsorption capacity and k_2 (g/mg h) calculated from the slope and intercept of plot
270 t/q_t versus t (Fig. 88 (b)). The constants k_2 and q_e determined from the model are shown in
271 Table 3 along with the corresponding correlation coefficients.

272 The intra-particle diffusion model can be given as [45]:

$$q_t = K_{di}t^{1/2} + C_i \quad (11)$$

273 where K_{di} is the rate constant for intra-particle diffusion model ($\text{mg g}^{-1}\text{h}^{-1/2}$) and the intercept,
274 C_i corresponds to the thickness of the adsorption layer (Fig. 8(c)). Intra-particle diffusion is
275 controlled by the diffusion of ions within the pores of the adsorbent [46].

276 Elovich equation is one of the most practical models for predicting chemisorption
277 processes, which can be expressed as [43, 47]:

$$q_t = \frac{1}{b} \ln(ab) + \frac{1}{b} \ln t \quad (12)$$

278 where a (mg g^{-1}) is the initial sorption rate and b ($\text{mg g}^{-1}\text{h}^{-1}$) is related to the extent of surface
279 coverage and activation energy for chemisorptions. The plot of the Elovich model is shown in
280 Fig. 8 (d). The $1/b$ value indicates the number of sites available for adsorption whereas the term
281 $1/b \ln(ab)$ is the adsorption magnitude when $\ln t$ is equal to zero; i.e., the adsorption quantity
282 when t is 1 h [48]. This value is useful in realizing initial adsorption behaviour [49]. Non-
283 linear regression was carried out on the kinetic data using equations 7, 9, 11, and 12. The model
284 parameters obtained from non-linear regression are given in Table 3. Values of determination
285 coefficient, R^2 , for both the pseudo-first and second-order models are > 0.990 , suggesting that
286 the models give a good fit. Similar trends were obtained for the Cr(VI) adsorption by dolomite
287 [11]. It was declared that the pseudo kinetic models are empirical equations that do not give a
288 precise understanding of the physio-chemical processes which are occurring.

289 However, the pseudo-first-order has the least SD value which implies that it provides a
290 better demonstration of the experimental data. On the other hand, for the pseudo-second-order,
291 it can be noted from Fig. 8 (b) that a better fit can be obtained by dividing the data into two
292 sections which can be representative of different modes of adsorption occurring on the dolomite
293 powder. Fig. 8 (c) also illustrates that the adsorption plots were not linear over the entire time

294 range and can be divided into two linear regions which validate that the adsorption is a multi-
295 stages process. The initial segment is regarded as a physisorption (i.e. ion exchange or surface
296 precipitation) and the second segment is attributed to the intra-particle diffusion effects [39].
297 Furthermore, the plots are linear in the initial stage of adsorption and the linearized data did
298 not pass through the origin signifying that intra-particle diffusion was not only the rate-limiting
299 step [37]. The Elovich equation also gave an acceptable fitting to the experimental data and
300 followed the pseudo second-order process. The Elovich model is suitable for systems with
301 heterogeneous adsorbing surfaces and suggests chemical adsorption processes with the
302 adsorption rate decreasing with time due to an increase in surface coverage [50].

303 **3.6. Comparison of adsorption capacity with various adsorbents**

304 The adsorption capacity of the fine dolomite determined in this study was compared with that
305 of other adsorbents adsorption capacities reported in the literature is shown in Table 4.
306 Dolomite material showed a higher adsorption capacity of phosphate than those of the reported
307 adsorbents. This may be attributed to the high initial phosphate concentration used, the
308 individual adsorbent characteristics and its ability to remove phosphate ions via precipitation
309 and ion exchange mechanisms [11]. It also suggests that dolomite is more applicable than the
310 other adsorbents for wastewater with a high phosphate concentration.

311 **4. Conclusion**

312 Fine dolomite was examined for the adsorption of phosphate from aqueous solutions. The
313 removal of phosphate from aqueous solutions was found to be significantly dependent on the
314 pH of the solution and ionic strength. The maximum adsorption capacity was achieved at pH
315 2. The monolayer adsorption capacity calculated from the Langmuir isotherm was obtained
316 227.3 mg P_g⁻¹ (optimum pH 2.0, ionic strength 0.0 M NaCl, 0.80 g L⁻¹ adsorbent mass,

317 temperature (20 °C) and 7 days contact time). The equilibrium isotherm data was accurately
318 described by the Redlich–Peterson isotherm model. The results show that fine dolomite is an
319 effective adsorbent for the removal and recovery of phosphate ions from aqueous solutions
320 under the tested experimental conditions.

321

322 **5. Reference**

- 323 [1] T. Ogata, S. Morisada, Y. Oinuma, Y. Seida, Y. Nakano, Preparation of adsorbent for
324 phosphate recovery from aqueous solutions based on condensed tannin gel, *Journal of*
325 *Hazardous Materials*, 192 (2011) 698-703.
- 326 [2] C. Mangwandi, A.B. Albadarin, G.M. Walker, S.J. Allen, Nutrient recovery form waste
327 water: optimization of adsorption process, *Chemical Engineering Transactions*, 24 (2011)
328 1177-1182.
- 329 [3] N. Karapinar, Application of natural zeolite for phosphorus and ammonium removal from
330 aqueous solutions, *Journal of Hazardous Materials*, 170 (2009) 1186-1191.
- 331 [4] N. Karapinar, E. Hoffmann, H.H. Hahn, P-recovery by secondary nucleation and growth of
332 calcium phosphates on magnetite mineral, *Water Research*, 40 (2006) 1210-1216.
- 333 [5] A. Ugurlu, B. Salman, Phosphorus removal by fly ash, *Environment International*, 24
334 (1998) 911-918.
- 335 [6] K. Suzuki, Y. Tanaka, T. Osada, M. Waki, Removal of phosphate, magnesium and calcium
336 from swine wastewater through crystallization enhanced by aeration, *Water Research*, 36
337 (2002) 2991-2998.
- 338 [7] P.M.J. Janssen, K. Meinema, R.H. F., *Biological Phosphorus Removal: Manual for Design*
339 *and Operation*, IWA Publishing, (2002) 11-13.
- 340 [8] A.B. Albadarin, C. Mangwandi, A.H. Al-Muhtaseb, G.M. Walker, S.J. Allen, M.N.M.
341 Ahmad, Modelling and Fixed Bed Column Adsorption of Cr(VI) onto Orthophosphoric Acid-
342 activated Lignin, *Chinese Journal of Chemical Engineering*, 20 (2012) 469-477.
- 343 [9] Y.A. Ouaisa, M. Chabani, A. Amrane, A. Bensmaili, Removal of tetracycline by
344 electrocoagulation: Kinetic and isotherm modeling through adsorption, *Journal of*
345 *Environmental Chemical Engineering*, 2 (2014) 177-184.
- 346 [10] G.K. Morse, S.W. Brett, J.A. Guy, J.N. Lester, Review: Phosphorus removal and recovery
347 technologies, *The Science of The Total Environment*, 212 (1998) 69-81.
- 348 [11] A.B. Albadarin, C. Mangwandi, A.a.H. Al-Muhtaseb, G.M. Walker, S.J. Allen, M.N.M.
349 Ahmad, Kinetic and thermodynamics of chromium ions adsorption onto low-cost dolomite
350 adsorbent, *Chemical Engineering Journal*, 179 (2012) 193-202.
- 351 [12] M.F. Abou Taleb, G.A. Mahmoud, S.M. Elsigeny, E.-S.A. Hegazy, Adsorption and
352 desorption of phosphate and nitrate ions using quaternary (polypropylene-g-N,N-
353 dimethylamino ethylmethacrylate) graft copolymer, *Journal of Hazardous Materials*, 159
354 (2008) 372-379.
- 355 [13] N.M. Agyei, C.A. Strydom, J.H. Potgieter, An investigation of phosphate ion adsorption
356 from aqueous solution by fly ash and slag, *Cement and Concrete Research*, 30 (2000) 823-826.
- 357 [14] M.Y. Can, E. Yildiz, Phosphate removal from water by fly ash: Factorial experimental
358 design, *Journal of Hazardous Materials*, 135 (2006) 165-170.
- 359 [15] M. Özacar, Phosphate adsorption characteristics of alunite to be used as a cement additive,
360 *Cement and Concrete Research*, 33 (2003) 1583-1587.
- 361 [16] L. Ruixia, G. Jinlong, T. Hongxiao, Adsorption of Fluoride, Phosphate, and Arsenate Ions
362 on a New Type of Ion Exchange Fiber, *Journal of Colloid and Interface Science*, 248 (2002)
363 268-274.
- 364 [17] A. Drizo, C.A. Frost, J. Grace, K.A. Smith, Physico-chemical screening of phosphate-
365 removing substrates for use in constructed wetland systems, *Water Research*, 33 (1999) 3595-
366 3602.
- 367 [18] E. Pehlivan, A.M. Özkan, S. Dinç, Ş. Parlayici, Adsorption of Cu²⁺ and Pb²⁺ ion on
368 dolomite powder, *Journal of Hazardous Materials*, 167 (2009) 1044-1049.

- 369 [19] A. Duffy, G.M. Walker, S.J. Allen, Investigations on the adsorption of acidic gases using
370 activated dolomite, *Chemical Engineering Journal*, 117 (2006) 239-244.
- 371 [20] S. Karaca, A. Gürses, M. Ejder, M. Açıklyıldız, Adsorptive removal of phosphate from
372 aqueous solutions using raw and calcinated dolomite, *Journal of Hazardous Materials*, 128
373 (2006) 273-279.
- 374 [21] S. Karaca, A. Gürses, M. Ejder, M. Açıklyıldız, Kinetic modeling of liquid-phase
375 adsorption of phosphate on dolomite, *Journal of Colloid and Interface Science*, 277 (2004) 257-
376 263.
- 377 [22] C. Mangwandi, A.B. Albadarin, L. JiangTao, S. Allen, G.M. Walker, Development of a
378 value-added soil conditioner from high shear co-granulation of organic waste and limestone
379 powder, *Powder Technology*, 252 (2014) 33-41.
- 380 [23] C. Mangwandi, L. JiangTao, A.B. Albadarin, S.J. Allen, G.M. Walker, Alternative method
381 for producing organic fertiliser from anaerobic digestion liquor and limestone powder: High
382 Shear wet granulation, *Powder Technology*, 233 (2013) 245-254.
- 383 [24] A.B. Albadarin, C. Mangwandi, G.M. Walker, S.J. Allen, M.N.M. Ahmad, M. Khraisheh,
384 Influence of solution chemistry on Cr(VI) reduction and complexation onto date-pits/tea-waste
385 biomaterials, *Journal of Environmental Management*, 114 (2013) 190-201.
- 386 [25] Jianyong Liu, Lihua Wan, Ling Zhang, Q. Zhou, Effect of pH, ionic strength, and
387 temperature on the phosphate adsorption onto lanthanum-doped activated carbon fiber, *Journal*
388 *of Colloid and Interface Science*, 364 490-496.
- 389 [26] Renkou XU, Yong WANG, Diwakar TIWARI, H. WANG, Effect of ionic strength on
390 adsorption of As(III) and As(V) on variable charge soils Original Research Article, *Journal of*
391 *Environmental Sciences*, 21 (2009) 927-932.
- 392 [27] B.H. Hameed, A.A. Rahman, Removal of phenol from aqueous solutions by adsorption
393 onto activated carbon prepared from biomass material, *Journal of Hazardous Materials*, 160
394 (2008) 576-581.
- 395 [28] L. Johansson, J.P. Gustafsson, Phosphate removal using blast furnace slags and opoka-
396 mechanisms, *Water Research*, 34 (2000) 259-265.
- 397 [29] M. Özacar, Contact time optimization of two-stage batch adsorber design using second-
398 order kinetic model for the adsorption of phosphate onto alunite, *Journal of Hazardous*
399 *Materials*, 137 (2006) 218-225.
- 400 [30] F.-C. Wu, R.-L. Tseng, R.-S. Juang, Kinetic modeling of liquid-phase adsorption of
401 reactive dyes and metal ions on chitosan, *Water Research*, 35 (2001) 613-618.
- 402 [31] S. Liodakis, G. Katsigiannis, T. Lympelopoulou, Ash properties of *Pinus halepensis*
403 needles treated with diammonium phosphate, *Thermochimica Acta*, 453 (2007) 136-146.
- 404 [32] L.A. Rodrigues, M.L.C.P. da Silva, Thermodynamic and kinetic investigations of
405 phosphate adsorption onto hydrous niobium oxide prepared by homogeneous solution method,
406 *Desalination*, 263 (2010) 29-35.
- 407 [33] H. Liu, X. Sun, C. Yin, C. Hu, Removal of phosphate by mesoporous ZrO₂, *Journal of*
408 *Hazardous Materials*, 151 (2008) 616-622.
- 409 [34] S. Moharami, M. Jalali, Removal of phosphorus from aqueous solution by Iranian natural
410 adsorbents, *Chemical Engineering Journal*, 223 (2013) 328-339.
- 411 [35] G. Zhang, H. Liu, R. Liu, J. Qu, Removal of phosphate from water by a Fe-Mn binary
412 oxide adsorbent, *Journal of Colloid and Interface Science*, 335 (2009) 168-174.
- 413 [36] S. Tanada, M. Kabayama, N. Kawasaki, T. Sakiyama, T. Nakamura, M. Araki, T. Tamura,
414 Removal of phosphate by aluminum oxide hydroxide, *Journal of Colloid and Interface Science*,
415 257 (2003) 135-140.
- 416 [37] T. Tuutijärvi, E. Repo, R. Vahala, M. Sillanpää, G. Chen, Effect of Competing Anions on
417 Arsenate Adsorption onto Maghemite Nanoparticles, *Chinese Journal of Chemical*
418 *Engineering*, 20 (2012) 505-514.

- 419 [38] J.B. Xiong, Q. Mahmood, Adsorptive removal of phosphate from aqueous media by peat,
420 Desalination, 259 (2010) 59-64.
- 421 [39] L.E. Katz, L.J. Criscenti, C.-C. Chen, J.P. Larentzos, H.M. Liljestrand, Temperature
422 effects on alkaline earth metal ions adsorption on gibbsite: Approaches from macroscopic
423 sorption experiments and molecular dynamics simulations, Journal of Colloid and Interface
424 Science, 399 (2013) 68-76.
- 425 [40] J. Antelo, M. Avena, S. Fiol, R. López, F. Arce, Effects of pH and ionic strength on the
426 adsorption of phosphate and arsenate at the goethite-water interface, Journal of Colloid and
427 Interface Science, 285 (2005) 476-486.
- 428 [41] S. Wang, X. Jin, Q. Bu, X. Zhou, F. Wu, Effects of particle size, organic matter and ionic
429 strength on the phosphate sorption in different trophic lake sediments, Journal of Hazardous
430 Materials, 128 (2006) 95-105.
- 431 [42] A. El Nemr, A. Khaled, O. Abdelwahab, A. El-Sikaily, Treatment of wastewater
432 containing toxic chromium using new activated carbon developed from date palm seed, Journal
433 of Hazardous Materials, 152 (2008) 263-275.
- 434 [43] B.H. Hameed, J.M. Salman, A.L. Ahmad, Adsorption isotherm and kinetic modeling of
435 2,4-D pesticide on activated carbon derived from date stones, Journal of Hazardous Materials,
436 163 (2009) 121-126.
- 437 [44] A.B. Albadarin, A.a.H. Al-Muhtaseb, N.A. Al-laqtah, G.M. Walker, S.J. Allen, M.N.M.
438 Ahmad, Biosorption of toxic chromium from aqueous phase by lignin: mechanism, effect of
439 other metal ions and salts, Chemical Engineering Journal, 169 (2011) 20-30.
- 440 [45] A.B. Albadarin, A.H. Al-Muhtaseb, G.M. Walker, S.J. Allen, M.N.M. Ahmad, Retention
441 of toxic chromium from aqueous phase by H₃PO₄-activated lignin: Effect of salts and
442 desorption studies, Desalination, 274 (2011) 64-73.
- 443 [46] T. Karthikeyan, S. Rajgopal, L.R. Miranda, Chromium(VI) adsorption from aqueous
444 solution by Hevea Brasilinesis sawdust activated carbon, Journal of Hazardous Materials, 124
445 (2005) 192-199.
- 446 [47] M. Özacar, I.A. Sengil, A kinetic study of metal complex dye sorption onto pine sawdust,
447 Process Biochemistry, 40 (2005) 565-572.
- 448 [48] Laleh Seifi, Ali Torabian, Hossein Kazemian, Golamreza Nabi Bidhendi, Ali Akbar
449 Azimi, Farshid Farhadi, S. Nazmara, Kinetic Study of BTEX Removal Using Granulated
450 Surfactant-Modified Natural Zeolites Nanoparticles, Water, Air, & Soil Pollution, 219 (2011)
451 443-457
- 452 [49] R.-L. Tseng, Mesopore control of high surface area NaOH-activated carbon, Journal of
453 Colloid and Interface Science, 303 (2006) 494-502.
- 454 [50] Feng-ChinWua, Ru-Ling Tsengb, R.-S. Juang, Characteristics of Elovich equation used
455 for the analysis of adsorption kinetics in dye-chitosan systems, Chemical Engineering Journal
456 150 (2009) 366–373.

457
458

459

460

461

462

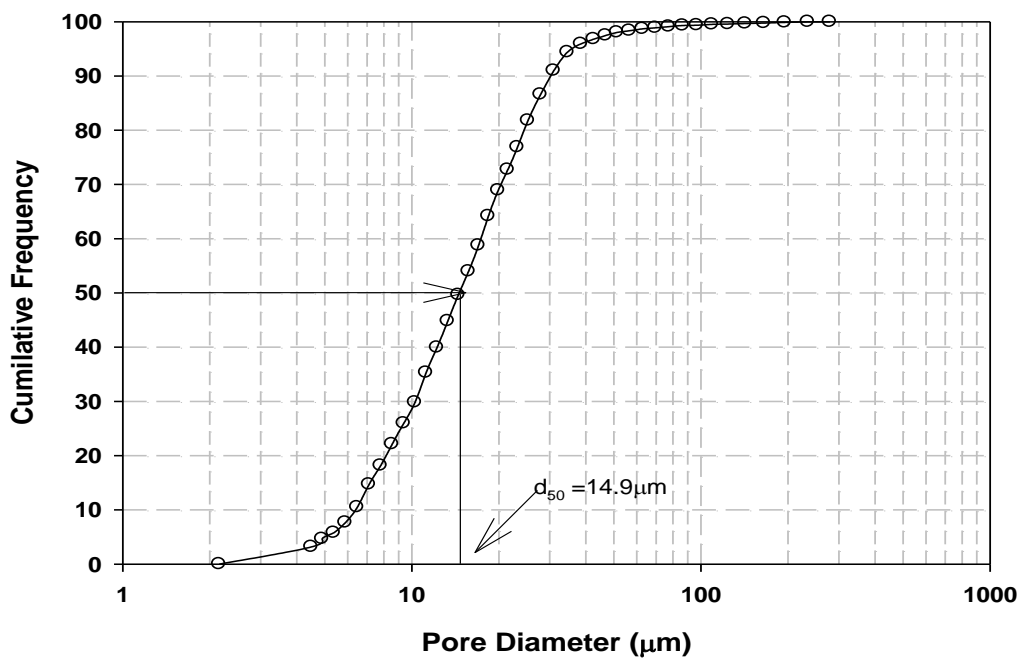
463

464

465

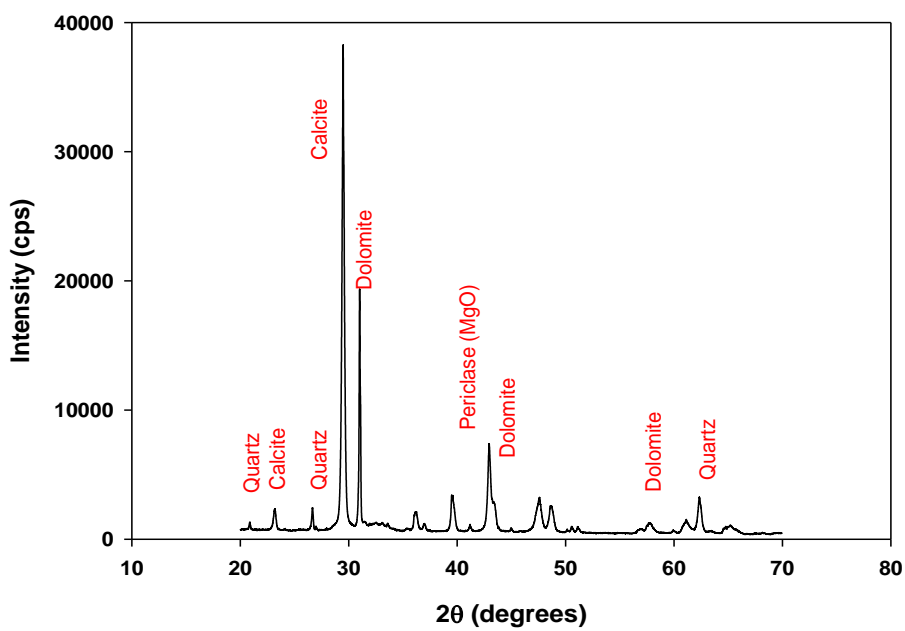
466

467 **Figures**

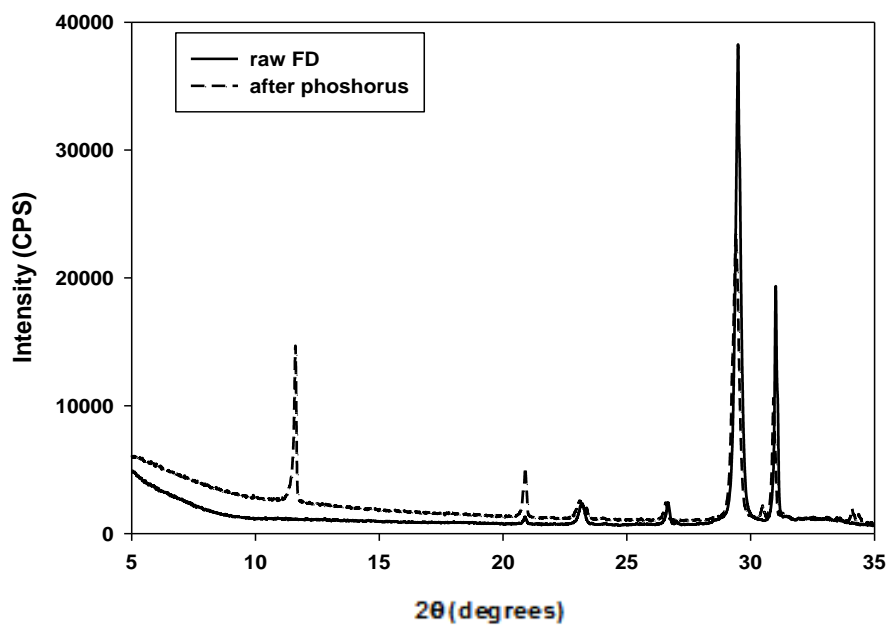


468

469 Fig. 1 : Cumulative pore size distribution curves of Fine Dolomite based on surface area.



(a)



(b)

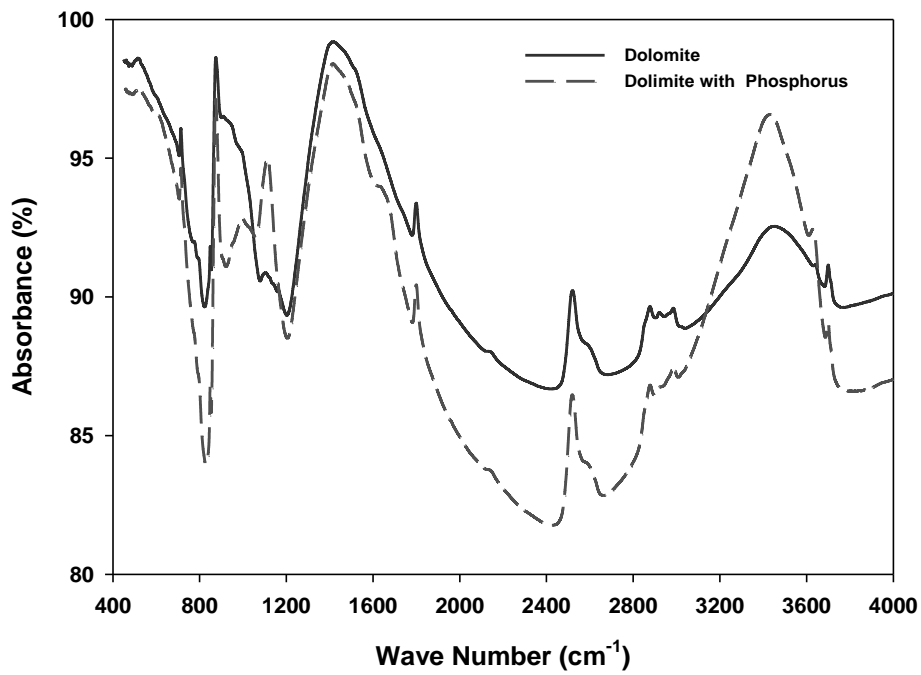
470

471 Fig. 2: XRD profiles of Fine Dolomite before (a) and after (b) adsorption of phosphate.

472

473

474



475

476 Fig. 3: FTIR spectrum of dolomite before and after phosphate adsorption.

477

478

479

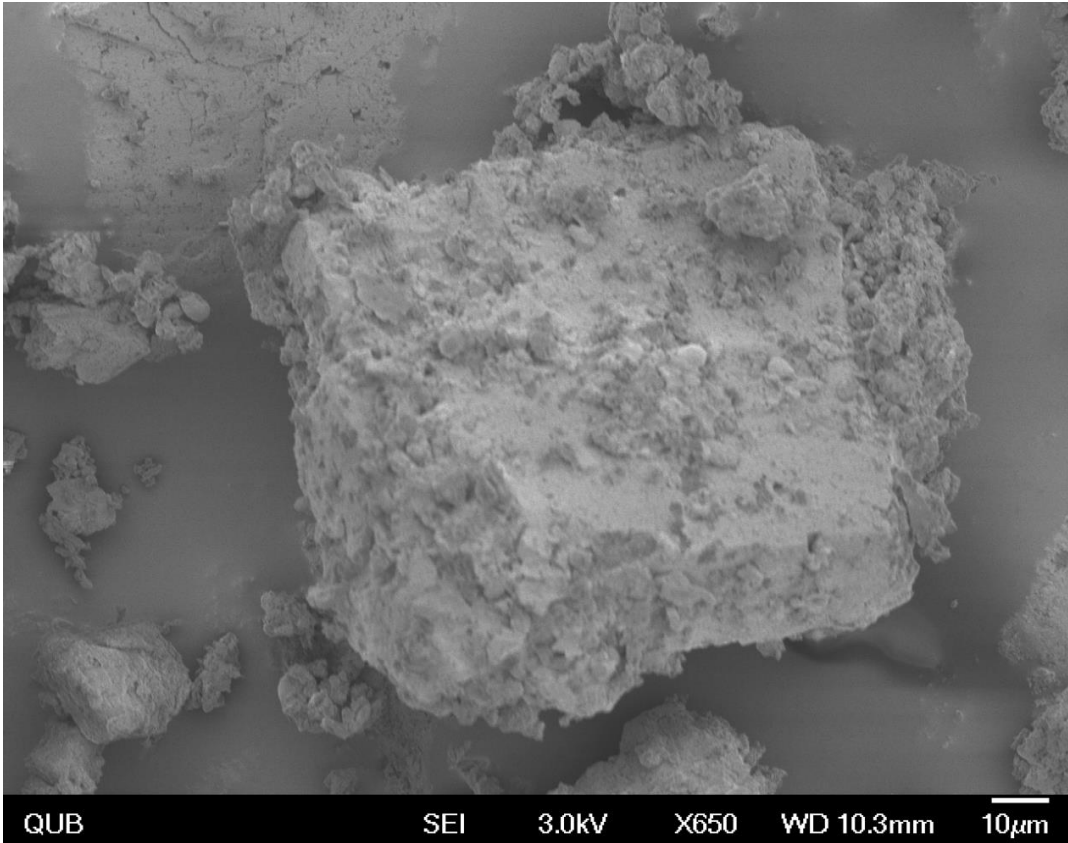
480

481

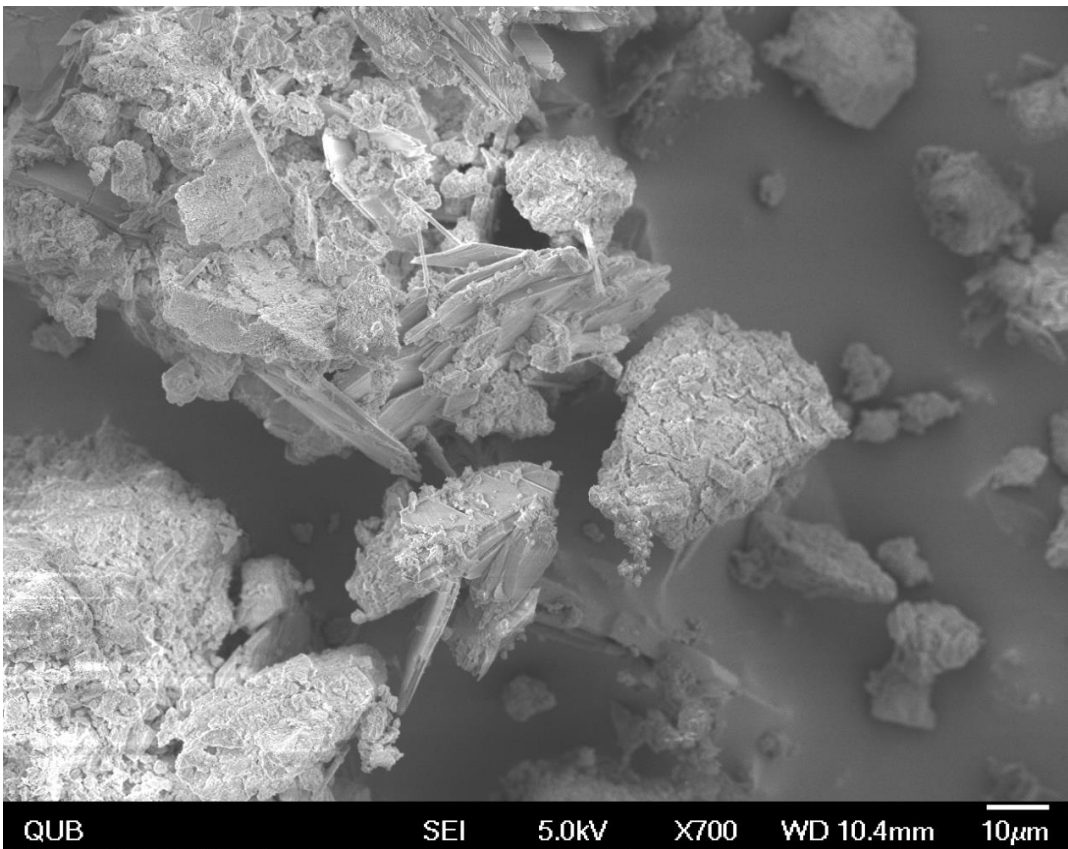
482

483

484

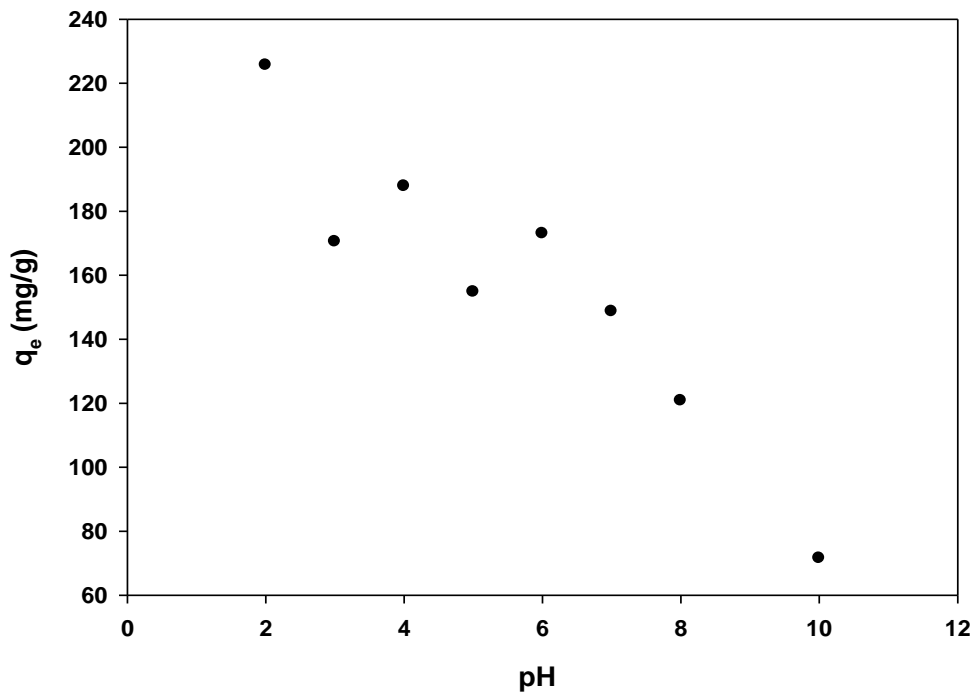


485



486

487 Fig. 4: The SEM micrographs of dolomite before and after phosphate adsorption.



488

489 Fig. 5: Effect of pH solution on the adsorption of phosphate ions onto fine dolomite adsorbent.

490

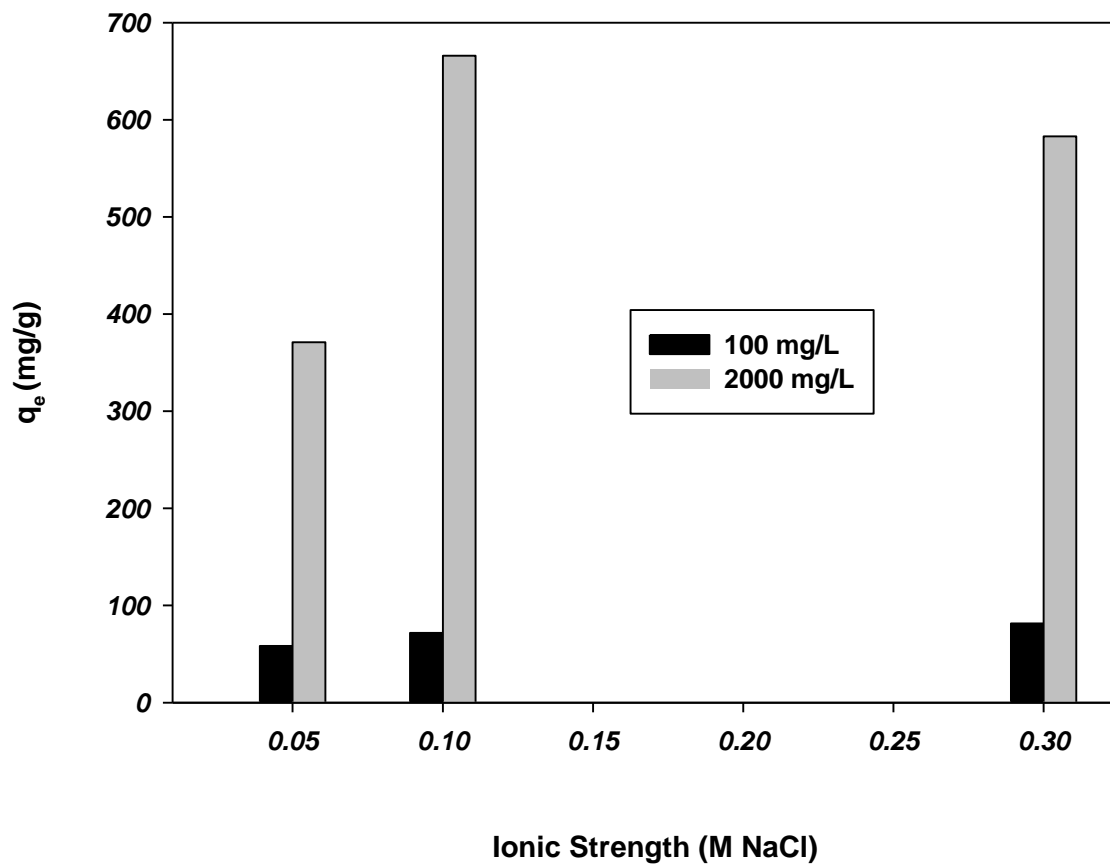
491

492

493

494

495



496

497

498 Fig. 6: Effect of ionic strength on adsorption of phosphate on fine dolomite.

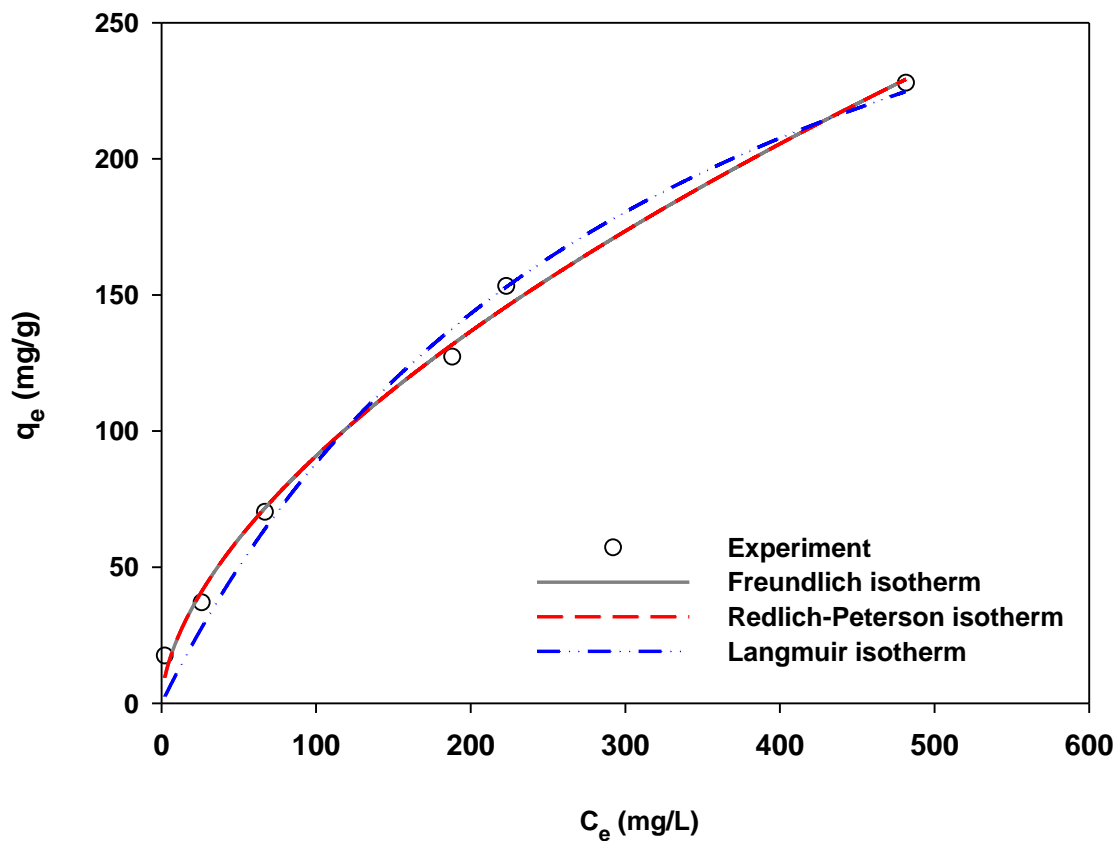
499

500

501

502

503



504

505 Fig. 7: Non-regression fits of Freundlich, Langmuir, Temkin and Redlich & Peterson models to the
 506 adsorption equilibrium data.

507

508

509

510

511

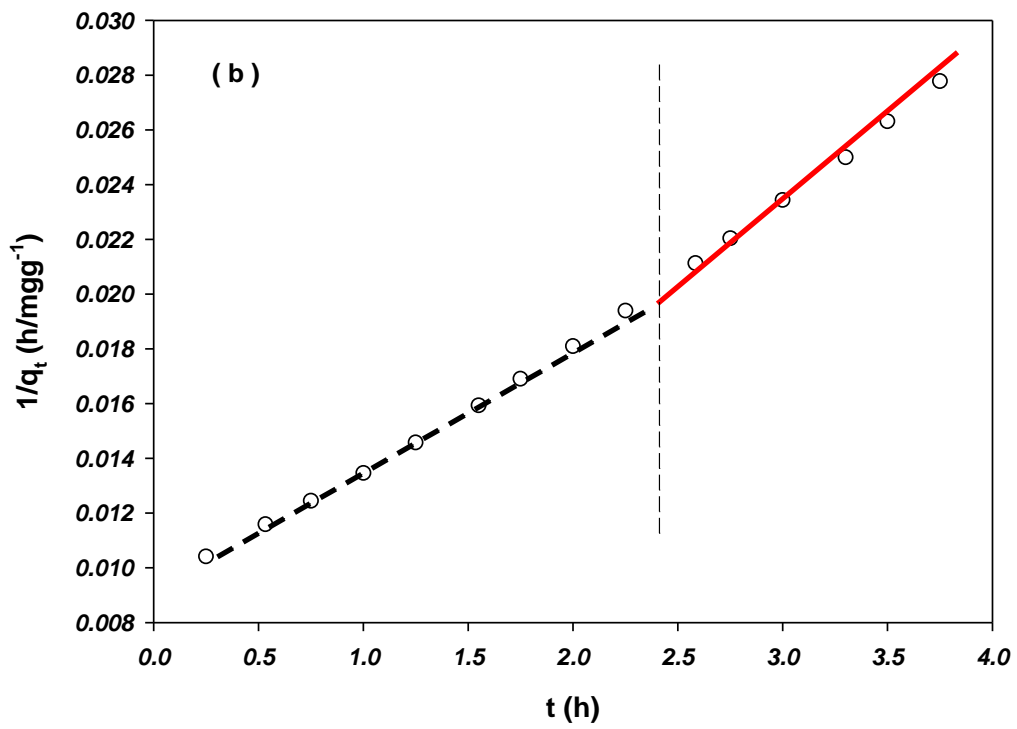
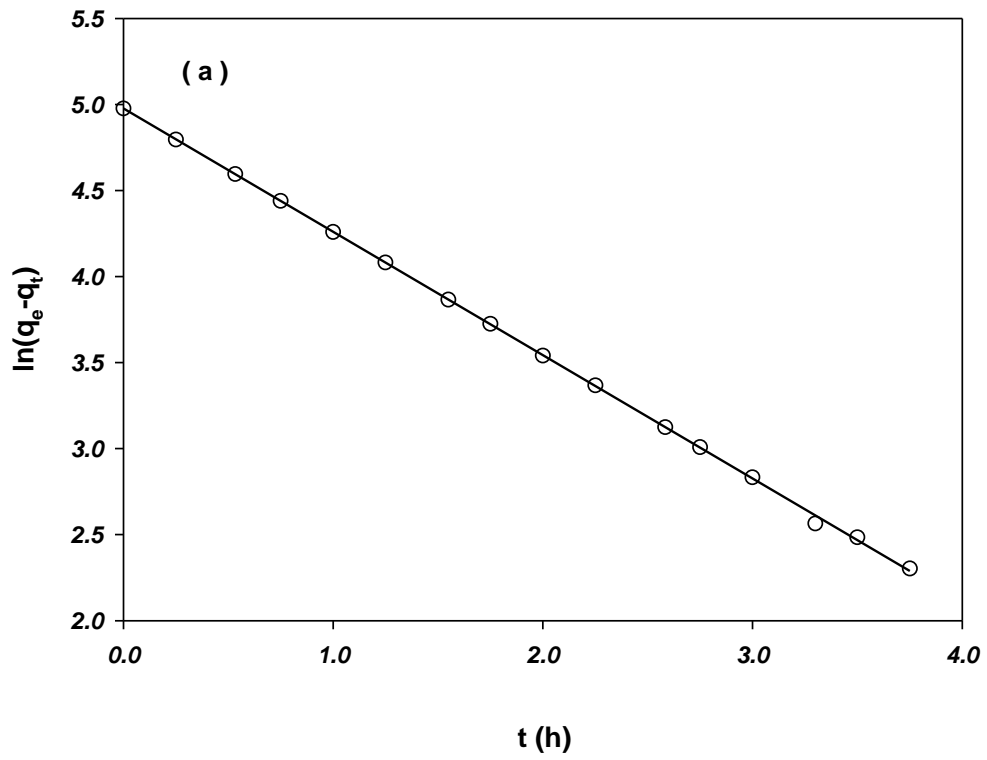
512

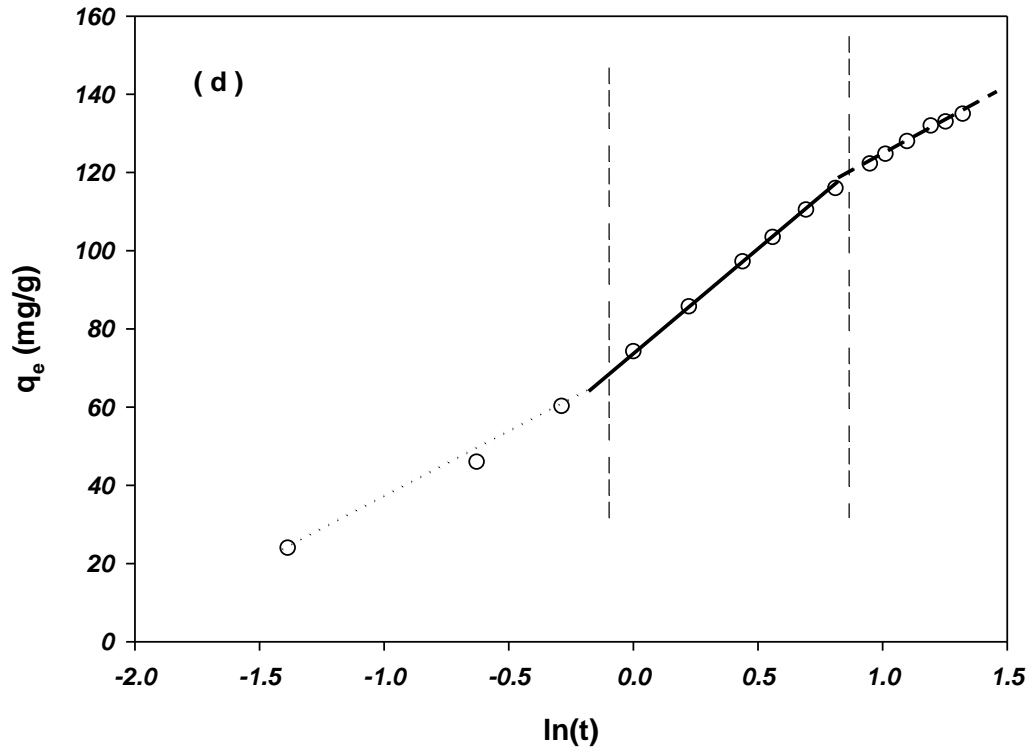
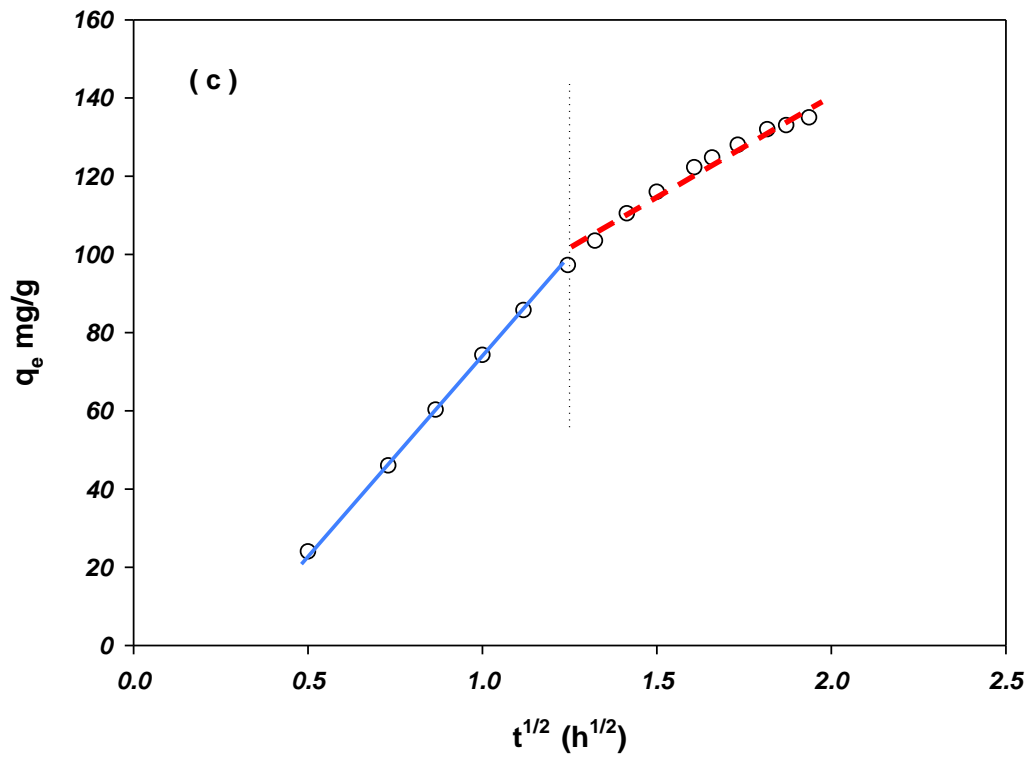
513

514

515

516





518

519 Fig. 8: Linearized plots of the different kinetic isotherms (a) Pseudo-first-Order (b) Pseudo-second-
 520 order Model (c) Intra-particle diffusion (d) Elovich equation.

521 **Tables**

522 Table 1: Quantitative composition of the fine Dolomite powder.

No.	Compound Name	Chemical Formula	SemiQuant (%)
1	Calcium Carbonate	CaCO ₃	68
2	Quartz	SiO ₂	9
3	Dolomite	CaMg(CO ₃) ₂	14
4	Periclase	MgO	9

523

524

525

526

527

528

529

530

531

532

533

534

535

536

537

538 Table 2: Summary of model parameters form non-linear regress fits of different isotherms to
 539 experimental data obtained at different ionic strength.

Isotherm	Parameter	NaCl Concentration			
		0.0 M	0.05 M	0.10 M	0.30 M
Freundlich	K_F	6.029	63.40	21.20	34.85
	n	1.698	3.432	2.015	2.420
	SD	0.216	1.450	0.870	1.480
	R^2	0.995	0.609	0.887	0.785
Langmuir	q_{\max}	377.8	616.8	984.9	851.0
	a_L	0.003	0.005	0.0023	0.003
	R_L	0.143	0.088	0.173	0.134
	SD	0.405	0.990	0.670	1.380
	R^2	0.985	0.759	0.938	0.587
	K_R	1.47×10^7	1.651	1.287	1.391
Redlich–Peterson	$a_R \times 10^{10}$	2.440	1.180	1.170	1.130
	β	0.411	0.271	0.323	0.326
	SD	0.344	0.450	0.380	1.000
	R^2	0.995	0.983	0.991	0.957

540

541

542

543 Table 3: Summary of the model parameters for the Kinetic models fitted to the kinetic data for
 544 adsorption of phosphate on fine dolomite.

545

Model	Parameter	
	k_1 (h ⁻¹)	0.716
Pseudo-first-order	q_e (mg P g ⁻¹)	145.0
	SD	0.003
	R^2	0.999
	k_2 (gm g ⁻¹ h ⁻¹)	0.003
Pseudo-second-order	q_e (mg g ⁻¹)	198.7
	SD	0.024
	R^2	0.999
	K_{di} (mg g ⁻¹ h ^{-0.5})	73.84
Intra particle diffusion	C_i (mg g ⁻¹)	1.25×10^{-11}
	SD	0.156
	R^2	0.999
	a	258.1
Elovich model	b	0.022
	SD	0.089
	R^2	0.996

546

547

548

549

550 Table 4: Comparison of adsorption capacities of the adsorbents.

Adsorbent	Adsorption capacity	pH	Max Conc. (mg/L)	Fit isotherm	Reference
Fine dolomite	377.8 (mg P/g)	2	2000	Redlich–Peterson	Current study
Iron-loaded tannin gel	31.3 (mg/g)	–	200	Freundlich	[1]
Alunite	4.69 (mol/g)	5	–	Langmuir	[15]
Mesoporous ZrO₂	29.7 (mg/g)	2–3	300	Langmuir	[30]
Fe–Mn binary oxide	36.0 (mg/g)	3	40.0	Freundlich/ Langmuir	[32]
Peat	8.91 (mg/g)	6.5	–	Langmuir	[35]

551

552